Applied Physics Letters PERSPECTIVE scitation.org/journal/apl

Perspective on the pressure-driven evolution of the lattice and electronic structure in perovskite and double perovskite

Cite as: Appl. Phys. Lett. **117**, 080502 (2020); doi: 10.1063/5.0014947
Submitted: 22 May 2020 · Accepted: 9 August 2020 ·
Published Online: 26 August 2020

Nana Li, Qian Zhang, Yonggang Wang, and Wenge Yang[a)]

AFFILIATIONS

Center for High Pressure Science and Technology Advanced Research (HPSTAR), Shanghai 201203, People's Republic of China

[a)]Author to whom correspondence should be addressed: yangwg@hpstar.ac.cn

ABSTRACT

Perovskite ABO_3 as one of the most common structures has demonstrated great structural flexibility and electronic applications. Evolving from perovskite, the typical double perovskite $A_2BB'O_6$ has two element species (B/B′), where the ordered arrangements of BO_6 and $B'O_6$ octahedron provide much more tunability. Especially, by applying external pressure, the energetic order between different phases in perovskite and double perovskite materials can be notably modified with more fascinating physical properties. However, it is still a challenge to propose a general model to explain and predict the high-pressure structures and properties of various perovskites and double perovskites due to their flexibility and complexity. In this perspective, we will discuss pressure effects on the crystalline structure and electronic configurations in some perovskites and double perovskites. We then focus on a prediction method for the evolution of the lattice and electronic structure for such materials with pressure. Finally, we will give a perspective on current challenges and opportunities for controlling and optimizing structural and electronic states of a given material for optimized functionalities.

Perovskite-type (Pv) oxides ABO_3 and double perovskite-type (dPv) oxides $A_2BB'O_6$ possess a wide variety of both scientifically and commercially physical properties depending on the choice of the constituting elements.[1–8] The ideal ABO_3 perovskite structures have a cubic symmetry, consisting of a framework of corner-sharing BO_6 octahedra with the A-type cation in each resulting cub-octahedral interstice and forming AO_{12} dodecahedron, as shown in Fig. 1(a). Double perovskite-type oxide $A_2BB'O_6$ is the evolution of ABO_3 in which the B site is occupied with two different atoms B/B′, and BO_6 and $B'O_6$ octahedral alternated with A atoms occupying the interstitial spaces, as shown in Fig. 1(b). The ordered arrangements of BO_6 and $B'O_6$ octahedron provide much more tunability on physical properties. For example, the double perovskite Sr_2FeMoO_6 shows the room-temperature magnetoresistance, promising for the development of ordered perovskite magnetoresistive devices that are operable at room temperature.[9] Lead free double perovskite La_2NiMnO_6 is a new promising material for photovoltaic applications.[10]

To accommodate different sizes of A and B/B′ cations, most Pv and dPv present flexible structures by rotation or tilting of the $B(B')O_6$ octahedrons,[11–16] as shown in Fig. 1. The stability of the Pv and dPv structures for the different A and B/B′ constituents is commonly discussed in terms of the Goldschmidt's tolerance factor (τ as defined below):[11,17]

$$\tau_{Pv} = (r_A + r_O)/\left(2^{1/2}(r_B + r_O)\right), \quad (1)$$

$$\tau_{dPv} = (r_A + r_O)/\left(2^{1/2}((r_B + r_{B'})/2 + r_O)\right), \quad (2)$$

where r_A, r_B, $r_{B'}$, and r_O are the ionic radii of the respective ions calculated from Shannon's ionic radii.[18] Ideal cubic perovskites usually hold τ value between 0.95 and 1.0 such as $CaSiO_3$ ($\tau_{Pv} = 0.99$) at room temperature and ambient pressure (RTAP).[13] When $0.75 < \tau_{Pv} < 0.95$, the Pv is distorted to orthorhombic, such as $REFeO_3$ (RE = rare earth, $\tau_{Pv} \sim 0.90$).[14] There are also various hexagonal non-Pv phases known with the ABO_3 stoichiometry and $\tau_{Pv} > 1$.[15,16] For dPv, the situation gets more complicated. The structure shows a huge difference even with a similar τ_{dPv} value. For instance, τ_{dPv} is 0.9789 for Ba_2YIrO_6 with a cubic structure, while the τ_{dPv} is 0.9792 for Sr_2ZnWO_6 with a tetragonal structure at RTAP.[19,20] In some cases, the dPv has the cubic structure at RTAP when the $\tau_{Pv} > 1$. For example, τ_{dPv} is 1.0380 and 1.0351 for ideal cubic Ba_2MgWO_6 and Ba_2ZnWO_6, respectively.[21] It was caused by the multiple element combinations at A and B/B′ sites.

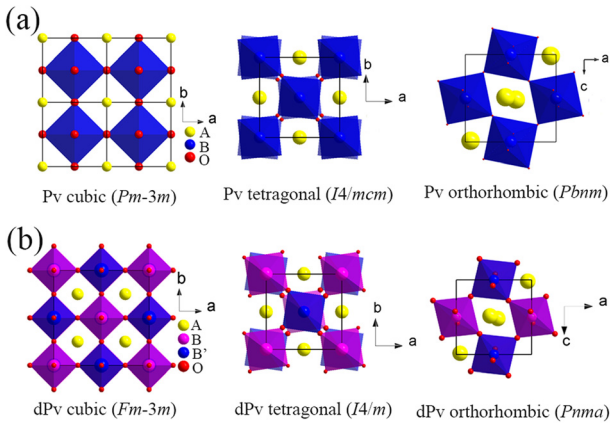

FIG. 1. The schematic representation of the crystal structure for perovskite (a) and double perovskite (b).

The distortions from the cubic symmetry give rise to changes in the physical properties that are important for the Pv and dPv applications.[22,23] For example, the intrinsic TiO_6 local bonding distortion and octahedral tilting in $CaTiO_3$ perovskite-based materials can modify intermediate energy states within the bandgap and associated photoluminescence emission profile.[22] Also, the high-T_c ferrimagnetism in Ca_2FeOsO_6 was driven by lattice distortion, which represents complex interplays between spins and orbitals.[23] Besides, as the predominant phase of the lower mantle and the most abundant mineral in Earth, the study on the orthorhombic $(Mg,Fe)SiO_3$ perovskite under extreme pressure and temperature leads to the discovery of the post-perovskite structure, which is considered as one of the most important events at the Earth's core–mantle boundary.[24,25]

The lattice distortion can be induced by many means. Among them, the external high pressure has been considered as a cleaner tool compared to other methods since it acts only on interatomic distances, which in turn modifies the material's mechanical and electronic properties.[26–38] For example, the pressure-induced magnetoelectric phase transition and the largest ferroelectric polarization among spin-driven ferroelectrics were reported in $TbMnO_3$.[29] Pressure-induced polymorphism and piezochromism were also studied in double perovskite Mn_2FeSbO_6.[37] $KNbO_3$ transformed from a ferroelectric orthorhombic *Cm2m* phase to another ferroelectric tetragonal *P4mm* phase at 7.0 GPa and then to a paraelectric cubic *Pm3m* phase at about 10.0 GPa.[39] Additionally, pressure can also redistribute the charge and melt the charge ordering via the structural phase transition. For example, at ambient pressure, $BiNiO_3$ crystallizes in the insulating phase (space group: *P*-1) with two ordered Bi valence (Bi^{3+}, Bi^{5+}) and Ni^{2+} valence occupation ($Bi^{3+}{}_{0.5}Bi^{5+}{}_{0.5}Ni^{2+}O_3$). At high pressure, by melting the charge ordering and disproportionation, the high-pressure phase (space group: *Pbnm*) turns to be metallic with different valence state ($Bi^{3+}Ni^{3+}O_3$).[38,40] What's more, in earth science, the structural properties of mantle phases, such as post-perovskite $(Mg,Fe)SiO_3$ under high pressure, are very important for understanding the enigmatic seismic features observed in the Earth's lower mantle down to the core–mantle boundary.[41–44] The ferromagnesian silicate $[(Mg,Fe)SiO_3]$ with nominally 10 mol. % Fe was found unstable under 95–101 GPa and 2200–2400 K and dissociated into an Fe poor orthorhombic phase and an Fe rich hexagonal phase, which suggests that the lower mantle may contain previously unidentified major phase.[43]

The structures of the Pv and dPv typically evolve in two ways under high pressure without breaking the polyhedron framework: tilting of the $B(B')O_6$ octahedra and polar cation displacement inside the $B(B')O_6$ or AO_{12} polyhedra.[45–51] For example, $BiFeO_3$ undergoes a phase transition at 3 GPa from a rhombohedrally distorted perovskite to a distorted monoclinic structure by the superimposition of tilts and cation displacements, and subsequent structural phase transition above 10 GPa from the distorted monoclinic structure to the nonpolar orthorhombic *Pnma* structure, as characterized by the cation displacements.[50,51]

For perovskite, there are several rules proposed to predict and explain the structural behavior under high pressure.[52–59] Based on the bond valence mechanism, Zhao *et al.* proposed that the AO_{12} dodecahedra are expected to be significantly more compressible than the BO_6 octahedral in orthorhombic perovskites, with both A and B cations having the formal charge +3 (3:3 perovskites) and the higher-symmetry structure should be expected at high pressure, but for perovskites with a +2 cation at the A site and a +4 cation at the octahedral B site (2:4 perovskites), they are predicted to become more distorted with pressure.[54] A majority of ABO_3 perovskites with non-magnetic elements at B site follows Zhao's rule.[60–64] For example, the distortion in the CaO_{12} and SnO_6 polyhedra and the octahedral SnO_6 tilting is attributed to the less compressible SnO_6 octahedron than CaO_{12} dodecahedron in site in $CaSnO_3$ (2:4 perovskite).[63] Also, they gave a general rule based on the ratios of the compressibility (M_A/M_B) of the AO_{12} and BO_6 polyhedra.[54] If $M_A/M_B > 1$, a transition to a higher-symmetry phase is expected under high pressure, whereas the opposite should occur when $M_A/M_B < 1$. For $LaAlO_3$, which has $M_A/M_B > 1$, its AlO_6 octahedra are therefore more compressible than the LaO_{12} sites and it undergoes a rhombohedral-to-cubic phase transition around 14 GPa.[60]

There are some exceptions like the strongly correlated systems that have strong electronic configuration effects under high pressure, such as Jahn–Teller (JT) systems.[65–72] For example, $LaMnO_3$ with an orthorhombic structure shows a complex behavior caused by the delocalization of electron states, which suppresses the JT effect of the MnO_6 octahedron but is insufficient to make the system metallic under high pressure.[67] It undergoes a transition to an unknown phase around 70 kbar because of the closing of the JT gap: the ionic Mn^{3+} species disappear and the system evolving toward a metallic-like phase is reached.[70] Another research also found that the total removal of the local JT distortion would occur only for pressures around 30 GPa in $LaMnO_3$, where metallization is reported to take place.[71] Besides, multiferroic material $BiFeO_3$, which has the strong tilt and polar distortions at room temperature, also exhibits a complex phase transition at high pressure caused by the changes in octahedron tilts and displacements of Bi^{3+} and Fe^{3+} cations.[50,51,72] Through absorption crystal-field spectroscopy, the linear redshift of both $4T^1$ and $4T^2$ Fe^{3+} bands was induced by high pressure, consistent with the compression of the FeO_6 octahedron under pressure.[72] Also, Fe^{3+} off-center displacements in FeO_6 still persist in the high-pressure phase (*Pnma*) for $BiFeO_3$.[72] In addition, $REFeO_3$ perovskites (RE = rare earth) show a spin transition of Fe^{3+} from high spin (HS) to low spin (LS) accompanied by a large volume collapse.[68,73] Therefore, the structure

configurations in strongly correlated perovskites will be more complex caused by the correlation between the lattice and electronic structures under high pressure.

How about dPvs, what's the general rule to predict the structural change for such materials under high pressure? Based on the element species, we divide dPvs into two types: One is the "weakly correlated electronic" (WCE) dPv in which the electronic structure does not strongly affect the lattice, and $B(B')O_6$ octahedra and AO_{12} polyhedra play a major role in determining distortions of the cation sites; the other is the "strongly correlated electronic" (SCE) dPv in which the lattice is strongly coupled with the spin, orbital, and valence. In this part, we try to explore whether there is a general rule to guide the structural change for WCE dPv under high pressure.

Because of the distribution in the valence state, a majority 4:8 dPv with a +2 alkali metal cation at the A site and a total +8 cation at the octahedral B and B′ sites are WCE dPv. Several high-pressure works have reported on such WCE dPv.[74–83] Basically, WCE dPvs tend to transform to a lower symmetry structure with the lattice distortion under high pressure, as shown in Fig. 2(a). For example, Ba_2YTaO_6 undergoes a structural phase transition from cubic to tetragonal with the onset of an octahedral tilting distortion about the *c* axis under high pressure.[74] Also, Ba_2BiTaO_6 transforms from rhombohedral with out-of-phase tilts about the [111] axis to the monoclinic structure with the [110] axis tilting around 4 GPa.[75] Experimental and theoretical studies on Sr_2CrReO_6 show a phase transition from cubic to tetragonal structure around 9 GPa.[76] Besides, Sr_2CoWO_6, Sr_2CaWO_6, and even Pb_2CoTeO_6 all show the structural phase transition toward a lower symmetry under high pressure.[77–79] In our previous work, we studied the structural phase transition of Sr_2ZnWO_6 under high pressure.[80] It also turns to a lower symmetry from monoclinic to triclinic at 9 GPa induced by the increasing of the distortion in the $Zn(W)O_6$ octahedron. Studies on other 4:8 WCE dPvs under high pressure have the similar trend to lower symmetry and more distortion of lattice.[80–83]

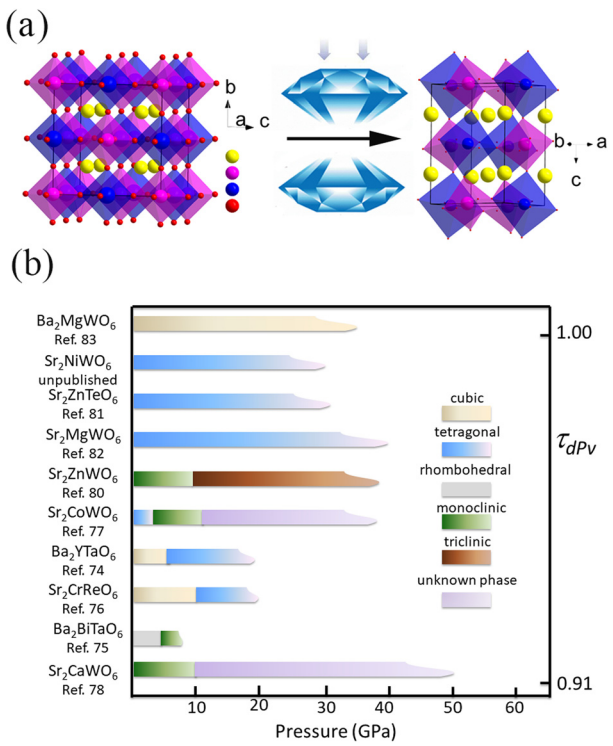

FIG. 2. (a) The schematic representation of the lattice distortion for WCE dPv under pressure. (b) Structure evolution of certain WCE double perovskites under pressure with different tolerance factors τ_{dPv}.

As summarized in Fig. 2(b), Sr_2ZnTeO_6[81] and Sr_2NiWO_6 (unpublished) remain stable up to 31 GPa with their ambient tetragonal structure. Both Ba_2MgWO_6 and Sr_2MgWO_6 also remain in their original phase under high pressure.[82] Let us take a look at the effect of one B site radius in Sr_2BWO_6 series: among Sr_2MgWO_6, Sr_2ZnWO_6, Sr_2CoWO_6, and Sr_2CaWO_6, Mg^{2+} has the smallest radius 0.72 Å, while Zn^{2+}, Co^{2+}, and Ca^{2+} have a larger radius as 0.74 Å, 0.75 Å, and 1.00 Å, respectively.[18] Sr_2BWO_6 (B = Zn, Co, and Ca) all undergo a structural phase transition at a pressure below 13 GPa, but Sr_2MgWO_6 remains in the ambient structure up to 31 GPa. We can conclude that the smaller B ion can keep the ambient structure sustainable to higher pressure. There has no enough data to compare the effect of the A site radius. However, we adopt the tolerance factor (τ_{dPv}) defined in Eq. (2) to quantitatively check the structure stability under pressure, in which we can simultaneously consider both A and B site radii. We draw a high-pressure structure diagram of some WCE double perovskites with their τ_{dPv}, as shown in Fig. 2(b). The larger the value of τ_{dPv}, the more stable the structure under high pressure. In contrast, with the smaller value of τ_{dPv}, the lattice is more prone to show the structural phase transition to low symmetry under high pressure. The smaller ion radius at the A site with small τ_{dPv} produces more space for the distorted $B(B')O_6$ octahedron under high pressure. For the smaller ion radius at the B(B′) site with a large τ_{dPv} value, it is easier to compress the $B(B')O_6$ octahedron and keep the lattice stable under high pressure. Therefore, the smaller the ion radius at the A site and the larger the ion radius at the B(B′) site, the much easier it is for such double perovskites to show a structural phase transition to lower symmetry under high pressure. In contrast, the larger the ion radius at the A site and the smaller the ion radius at the B(B′) site, the crystal structure of such double perovskite is easier to remain stable.

For perovskite predicting models at high pressure, there are not only qualitative but also quantitative method, which shows the detailed distortion of perovskite structures as a function of pressure. There are some excellent works that have been successfully applied to some perovskites, such as $CaTiO_3$, $CaSnO_3$, and $MgSiO_3$.[54,84] For WCE dPv, we try to build a simple model for quantitatively investigating the lattice evolution at high pressure, only using ambient-pressure crystal structure data and the unit-cell parameters. First, we introduced a modified factor: the local instability index (LII), which is derived from the bond valence sums at the cation sites alone:[84]

$$LII = \left[\frac{(\Delta V_A)^2 + (\Delta V_B)^2 + (\Delta V_{B'})^2}{3}\right]^{1/2}, \quad (3)$$

where ΔV_A, ΔV_B, and $\Delta V_{B'}$ are the difference of the bond valence sums at the cation sites for the fractional atomic coordinates of a model structure at pressure *P* and the ambient-pressure structure at ambient pressure.[84] ΔV_A, ΔV_B, and $\Delta V_{B'}$ can be obtained by SPuDS program.[85]

Here, we used "fixed coordinate" model to calculate the *LII* values under high pressure for such dPv, which are only based upon the

knowledge of the ambient-pressure structure and the unit-cell parameters at high pressures. The *LII* values at high pressure for some WCE dPv are shown in Fig. 3(a). Obviously, the *LII* values all become greater with increasing pressure for such dPv whether the samples have phase transition or not. Hereupon, we define a new factor "compromise instability index" (*CII*), which is derived from the difference of the bond valence sums in A and B/B′ sites,

$$CII_i = \left(V_{Bi}(\text{calc}) - V_B(\text{ox})\right)^2 + \left(V_{B'i}(\text{calc}) - V_{B'}(\text{ox})\right)^2 - 4*\left(V_{Ai}(\text{calc}) - V_A(\text{ox})\right)^2, \quad (4)$$

where *Vi*(*ox*) is the formal valence (equal to its oxidation state) and *Vi*(*calc*) is the calculated bond valence sum for the A, B, and B′ ions at pressure *Pi*. *Vi*(*calc*) can be obtained by SPuDS program[85] using the "fixed coordinate" model.

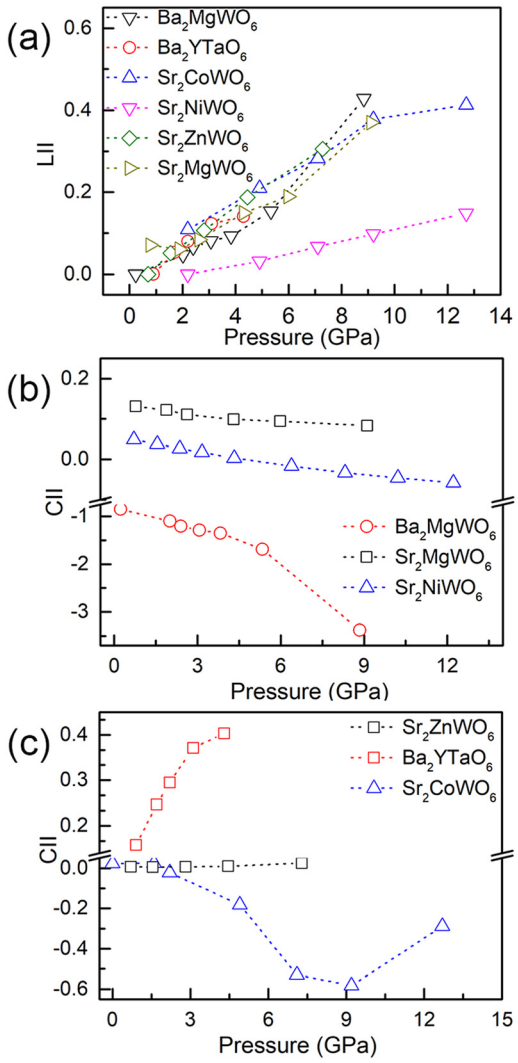

FIG. 3. (a) The change of *LII* values of Ba_2MgWO_6, Ba_2YTaO_6, Sr_2CoWO_6, Sr_2NiWO_6, and Sr_2ZnWO_6 under high pressure. (b) is the pressure dependence of *CII* for Ba_2MgWO_6, Sr_2MgWO_6, and Sr_2NiWO_6. (c) is the pressure dependence of *CII* for Sr_2ZnWO_6, Ba_2YTaO_6, and Sr_2CoWO_6.

Then, we gave the *CII* values with pressure for those WCE dPvs, as shown in Figs. 3(b) and 3(c). The compromise instability index *CII* is more inclined to decrease ($dCII/dP < 0$) for WCE dPv, which has no structural phase transition under high pressure; in contrast, *CII* is more inclined to increase ($dCII/dP > 0$) for WCE dPv, which has structural phase transition under high pressure. For Ba_2MgWO_6, Sr_2MgWO_6, and Sr_2NiWO_6 in which the crystal structure is stable within the pressure range of the study, *CII* decrease with increasing pressure. However, *CII* increases with pressure for Sr_2ZnWO_6 and Ba_2YTaO_6, in which the structural phase transition occurs around 10 GPa and 5 GPa, respectively. For Sr_2CoWO_6, it shows two structural phase transitions around 2 GPa and 12 GPa. Although *CII* decreases in the intermediate pressure range of two phase transitions, it still increases near the phase transition point. Therefore, the compromise instability index *CII* can be used as an important parameter to judge whether there is phase transition or not for WCE dPv at high pressure.

In the strongly correlated electronic (SCE) Pv and dPv in which the lattice is strongly coupled with the spin, orbital, or valence, the high-pressure behaviors become more complicated.[86–91] It will induce more significant physical properties such as the charge transfer, insulator-to-metal transition, magnetic transition, and even non-fermi liquid behavior. For instance, $Ba_2PrRu_{0.8}Ir_{0.2}O_6$ shows an unusual lattice change under high pressure, in which a structural phase transition from monoclinic to tetragonal is driven by the charge transfer from Pr^{3+} to Pr^{4+} with pressure.[91] Besides, compression on Sr_2FeOsO_6 drives an unexpected transition from the antiferromagnetic to ferrimagnetic order, accompanied by the lattice stable up to 56 GPa.[92,93] It was caused by the increase in the crystal-field splitting at Os^{5+} sites rather than by bending of the Fe–O–Os bonds.[92,93] What's more, the magnetic transition temperature is largely and slightly enhanced for Ba_2FeMoO_6 and Sr_2FeMoO_6, respectively.[86] Sr_2FeMoO_s also shows a metal–insulator transition caused by the compression of the unit cell around 2.1 GPa.[87] Especially, $PrNiO_3$ shows an insulator to metal transition with the transforming to a non-Fermi-liquid phase with pressure, which is caused by both lattice and spin fluctuations where the transition temperature $T_{IM} = T_N$ is terminated.[94] The similar phenomenon was also discovered in other $RENiO_3$ (RE = rare earth) at high pressure.[95]

The transition metals, such as Fe^{3+}/Fe^{2+} and Mn^{3+} in SCE systems, show novel and interesting high-pressure behaviors because of the correlation among the lattice, spin, and orbital, which leads to strong modification on the magnetic, electronic, optical, and other properties in the corresponding systems. Especially, the pressure-induced spin transition occurred from high spin to low spin for such transition metal largely correlates with the lattice and electronic properties. For instance, in $LaFeO_3$, the spin transition of Fe^{3+} accompanied by the lattice collapse occurs at around 50 GPa.[67] Concurrent of the HS to LS transition and lattice collapse during structural phase transition has been observed in other systems.[96–98] Also, they show some interesting pressure-induced spin crossover phenomenon that have not been discovered yet in perovskite and double perovskite oxides. For instance, the spin crossover of Fe^{2+} can induce the superconducting in $FePSe_3$ under high pressure.[96] What's more, a high-to-low spin crossover of Fe^{2+} in $CuFeS_2$ is manifested along with the structural phase transition and a surprising *n*-type semiconductor to

p-type semiconductor transition with pressure.[98] The study and prediction on the pressure-induced spin crossover of dPv oxides can give an opportunity to produce such unusual electronic states and interesting physical properties.

In this part, we mainly discuss the correlation between the lattice and spin configurations in SCE dPv under high pressure. In general, the spin crossover in these transition metals is caused by the *d*-orbital splitting with pressure. We gave a schematic *d*-orbital splitting diagram of Fe^{3+} in the FeO_6 octahedra under high pressure, as shown in Fig. 4(a). The net spin magnetic moment of transition metals in the $B(B')O_6$ octahedron in SCE double perovskites is mainly controlled by the competition between the crystal-field splitting Δ_{cf} (favorite for the LS state) and the intra-atomic Hund's exchange term *J* (favorite for the HS state). Δ_{cf} is sensitive to external pressure, which will promote the crystal field splitting and then induce the spin transition of such ions and finally strongly influence the electronic and magnetic properties of SCE dPv. For Sr_2FeMoO_6, a spin crossover of Fe ion from high-spin to low-spin state is found accompanied by a transition from the ferrimagnetic half-metallic to nonmagnetic semiconductor state.[87,88] Another

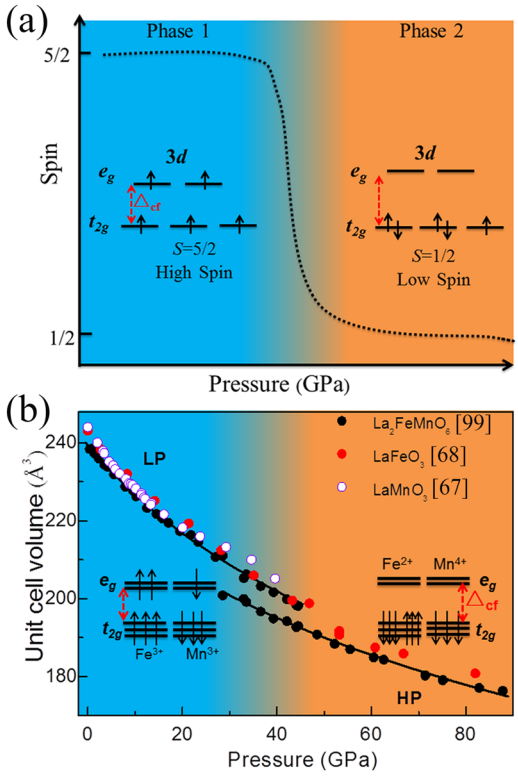

FIG. 4. (a) A schematic *d*-orbital splitting diagram for Fe^{3+} in the FeO_6 octahedra with pressure. (b) The high-pressure behavior of La_2FeMnO_6,[99] $LaFeO_3$,[68] and $LaMnO_3$.[67] For $LaMnO_3$, reproduced with permission from Loa *et al.*, Phys. Rev. Lett. **87**, 125501 (2001).[67] Copyright 2001 American Physical Society. For $LaFeO_3$, reproduced with permission from Xu *et al.*, Phys. Rev. B **64**, 094411 (2001).[68] Copyright 2001 American Physical Society. For La_2FeMnO_6, reproduced with permission from Li *et al.*, Phys. Rev. B **99**, 195115 (2019).[99] Copyright 2019 American Physical Society.

theoretical study on La_2VMnO_6 shows that Mn^{3+} experiences a transition from the high spin state ($t_{2g}^3e_g1$) to low spin state (t_{2g}^4), making La_2VMnO_6 a half-metallic ferrimagnet accompanied by the volume collapse under some critical pressure.[89]

To date, most studies of double perovskites have only one transition metal involved in spin transition. How about the interplay of double-spin crossover with two transition metals? Is there a possible charge transfer involving in the double-spin crossover to minimize the overall energy? To check all these questions, we studied the high-pressure structure of La_2FeMnO_6, and monitored the spin and valence status of Fe and Mn at the B-site.[99] Unlike $LaMnO_3$ and $LaFeO_3$,[67,68,100] La_2FeMnO_6 shows a double-spin crossover behavior under high pressure. The strong coupling between Fe and Mn leads to a combined valence/spin transition: $Fe^{3+}(S=5/2) \rightarrow Fe^{2+}(S=0)$ and $Mn^{3+}(S=2) \rightarrow Mn^{4+}(S=3/2)$, with an isostructural phase transition under high pressure, as shown in Fig. 4(b).

However, in La_2FeMnO_6, the randomly distributed Fe/Mn leads to a "diffuse pressure-induced phase transition," a structural transformation over a broad pressure range, without a well-defined critical pressure point. So both lattice and spin transitions spread out over a large pressure range with different configurations at each pressure stage in La_2FeMnO_6. This phenomenon is not conducive to the practical application of such a material because of the broad pressure range for the structural transformation. To avoid this problem, we can design an ordered B/B′ site in dPv and choose different transition metal combinations such as Fe/Co, Co/Mn, and Co/Cr that may undergo a double spin transition, and the pronounced spin–orbit coupling between two transition metals may provide more options for designing novel spintronic materials with tailored properties.[101–103] For instance, the theoretical studies on Sr_2FeCoO_6 show that Co^{4+}/Fe^{4+} in the high spin states can lead to its metallicity and ferromagnetism.[101] Then, the spin transition of Co^{4+}/Fe^{4+} will give a huge change in their electronic and magnetic properties with pressure. Besides, the system will become more complex if the $B(B')O_6$ octahedra involve orbitally degenerate transition metal ions (B/B′: Cu^{2+}, Cr^{2+}, Fe^{2+}, Mn^{3+}, Ni^{3+}, or Co^{3+}). The JT coupling induces low-symmetry $B(B')O_6$ distortions, which are eventually responsible for the striking properties related to both the orbital ordering and JT distortion.[102] For instance, JT distortions of the MnO_6 octahedra in $La_{0.85}MnO_{3-\delta}$ will induce the reduction in the metal–insulator transition temperature at high pressure.[103] Also, the coherence length of the JT distortions in $La_{3/4}Ca_{1/4}MnO_3$ induced a structural modification with high pressure.[104] In $RENiO_3$, the localized electrons of Ni undergo a cooperative JT distortion but stronger Ni–O bonding in alternate $NiO_{6/2}$ octahedra creates molecular *e* orbitals within the more strongly bonded clusters.[105] All these induce the approach to crossover to itinerant-electron behavior from the localized-electron side.[105] Besides, high-pressure research on Cu^{2+} and Mn^{3+} showed that JT distortion reduced upon compression and is eventually suppressed at pressures above 20 GPa.[67,102–106] If we combine the transition metals in B/B′, which contains both JT distortion and spin crossover, it will induce amazing physical properties at high pressure. For instance, the intermediate spin states of Mn^{3+}/Co^{3+} can lead to JT distortions where the JT ion will have a single e_g electron and the double degeneracy of e_g state will be lifted with pressure. This will lead to itinerant behavior of the single electron, which will contribute to the magnetic and transport properties.[107,108]

Here, we established a general rule among the tolerance factor τ, compromise instability index *CII* and the stability of the crystal structure in the 4:8 WCE double perovskites under high pressure. The correlation among the lattice and spin in some SCE dPvs was discussed comprehensively.

For Pv and dPv with polar non-centrosymmetric, ferroelectrics has been extensively studied for potential applications in room-temperature pyroelectric infrared detectors and electronic and photonic devices.[109–111] Currently, the pressure effect is still not quite clear. For instance, what is the major contribution from the octahedral tilting and the polar cation displacements with pressure, and whether the ferroelectricity can be indeed enhanced or reappeared at high pressure for such materials? Further research is needed on the evolution of the lattice correlated with the electronic structure for such Pv and dPv under high pressure.

This review only involves two types of structures: ABO_3 or $A_2BB'O_6$. Oxygen-deficiency in Pv and dPv could provide another way to modify the structure and valence status, and their pressure responses. One typical oxygen-deficient perovskite $A_2B_2O_5$ differs in the ordering patterns of anion vacancies. These compounds crystallize in the brownmillerite-type (B-type) structure consisting of alternating layers of corner-sharing BO_6 octahedra and corner-sharing BO_4 tetrahedral, as shown in Fig. 5(a).

Under high pressure, the B-type structure prefers to transform to the perovskite-type (P-type) structure because of the breaking and forming of B–O–B bonds in the octahedral and adjacent tetrahedral B–O layers of the brownmillerite-type structure. For example, $Sr_2Fe_2O_5$ shows a structural phase transition from the B-type structure (space group *Ibm*2) to a tetragonal perovskite-like structure with oxygen-deficient at 15 GPa, while $SrFeO_3$ remains in its cubic structure up to 56 GPa.[112–114] One can directly synthesize the tetragonal perovskite-like structure of $Sr_2V_2O_5$ with a large volume press under high pressure and temperature conditions (unpublished). The tetragonal phase of $Sr_2V_2O_5$ can sustain a pressure of up to 40 GPa. Another high-pressure study on $Ca_2Fe_2O_5$ shows that it remains B-type structures up to 10 GPa.[115] We predict that it will transform to the perovskite-like structure with a higher pressure. However, further experiments are called in to confirm these predictions. The equations of state for $CaFeO_{2.5}$, $SrVO_{2.5}$, $SrFeO_{2.5}$, and $SrFeO_3$ are displayed in Fig. 5(b) for comparison.

Double perovskite can be derived to other forms such as $AA'_3B_4O_{12}$-type and $AB_{2/3}B'_{1/3}O_3$-type according to the different atomic ratios in the A or B site. For example, the A-site-ordered double perovskite $LaCu_3Fe_4O_{12}$ adopts a cubic structure, where the Cu ions at the A site make the square-planar AO_4 units and the Fe ions at the B site form corner-sharing BO_6 octahedra.[116,117] Under external pressure, a phase transition occurs along with a significant volume collapse and charge transfer between Cu and Fe, which leads to a surprising electric/magnetic property change from an antiferromagnetic insulating state to a paramagnetic metallic state.[117] $In_3Cu_2VO_9$ with $AB_{2/3}B'_{1/3}O_3$ type adopts the honeycomb-lattice structure, which consists of alternating layers of InO_6 octahedra, and Cu^{2+} and V^{5+} ions in the trigonal–bipyramidal coordination.[118] In the new cuprate $La_4Cu_3MoO_{12}$, the Cu and Mo are coordinated by O in the corner-sharing trigonal bipyramids that are sandwiched between layers of lanthanum cations.[119] In these specific derivative double perovskites, the transition metals can occupy the lattice in very rich ways, which may induce more advanced mechanical and electronic properties under high pressure. However, the high-pressure research on such complexed derivative double perovskites is still rare. It is still a challenge task to fully understand the mechanism of the lattice evolution with the electronic configuration of such dPv under high pressure and optimize the functionality and achieve the intriguing properties.

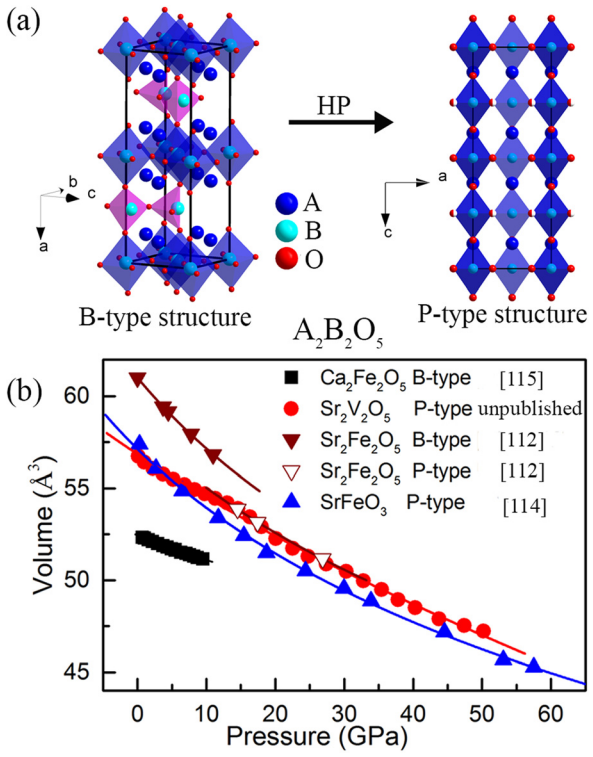

FIG. 5. (a) The structure changes from the brownmillerite (B)-type structure to the perovskite (P)-like structure for $A_2B_2O_5$ under high pressure. Half-red O atoms have an occupancy of 1/2 in the perovskite (P)-like structure. (b) The volume of a primitive perovskite-type unit cell as a function of pressure for $Ca_2Fe_2O_5$,[115] $Sr_2V_2O_5$, $Sr_2Fe_2O_5$,[112] and $SrFeO_3$.[114] For $Sr_2Fe_2O_5$, reproduced with permission from Adler *et al.*, J. Solid State Chem. **155**, 381–388 (2000).[112] Copyright 2000 Elsevier. For $SrFeO_3$, reproduced with permission from Kawakami *et al.*, J. Phys. Soc. Jpn. **72**, 33–36 (2003).[114] Copyright 2003 Physical Society of Japan. For $Ca_2Fe_2O_5$, reproduced with permission from Ross *et al.*, Phys. Earth Planet. Inter. **129**, 145–151 (2002).[115] Copyright 2002 Elsevier.

This work was financially supported by the National Natural Science Foundation of China (Grant Nos. U1930401, 51527801, and 51772184).

DATA AVAILABILITY

The data that support the findings of this study are available from the corresponding author upon reasonable request.

REFERENCES

[1]S. Valencia, A. Crassous, L. Bocher, V. Garcia, X. Moya, R. O. Cherifi, C. Deranlot, K. Bouzehouane, S. Fusil, A. Zobelli, A. Gloter, N. D. Mathur, A. Gaupp, R. Abrudan, F. Radu, A. Barthélémy, and M. Bibes, Nat. Mater. **10**, 753–758 (2011).

[2]L. H. Yin, J. Yang, R. R. Zhang, J. M. Dai, W. H. Song, and Y. P. Sun, Appl. Phys. Lett. **104**, 032904 (2014).
[3]S. Sharma, J. Saha, S. D. Kaushik, V. Siruguri, and S. Patnaik, Appl. Phys. Lett. **103**, 012903 (2013).
[4]J. Cong, K. Zhai, Y. Chai, D. Shang, D. D. Khalyavin, R. D. Johnson, D. P. Kozlenko, S. E. Kichanov, A. M. Abakumov, A. A. Tsirlin, L. Dubrovinsky, X. Xu, Z. Sheng, S. V. Ovsyannikov, and Y. Sun, Nat. Commun. **9**, 2996 (2018).
[5]A. Maignan, C. Martin, O. Lebedev, J. Sottmann, L. Nataf, F. Baudelet, S. Hébert, and R. E. Carbonioc, Chem. Commun. **55**, 5878–5881 (2019).
[6]Y. Bai, T. Siponkoski, J. Peräntie, H. Jantunen, and J. Juuti, Appl. Phys. Lett. **110**, 063903 (2017).
[7]J. Cai, C. Wang, B. Shen, J. Zhao, and W. Zhan, Appl. Phys. Lett. **71**, 1727 (1997).
[8]Y. Du, Z. X. Cheng, S. X. Dou, X. L. Wang, H. Y. Zhao, and H. Kimura, Appl. Phys. Lett. **97**, 122502 (2010).
[9]K.-I. Kobayashi, T. Kimura, H. Sawada, K. Terakura, and Y. Tokura, Nature **395**, 677–680 (1998).
[10]M. S. Sheikh, D. Ghosh, A. Dutta, S. Bhattacharyya, and T. P. Sinha, Mater. Sci. Eng.: B **226**, 10–17 (2017).
[11]V. M. Goldschmidt, Naturwissenschaften **14**, 477–485 (1926).
[12]D. Yang, W. Wang, T. Yang, C. I. Lampronti, H. Ye, L. Wu, Q. Yu, and S. Lu, APL Materials **6**, 066102 (2018).
[13]L. Liu and A. E. Ringwood, Earth Planet. Sci. Lett. **28**, 209–211 (1975).
[14]A. Wu, G. Cheng, H. Shen, J. Xu, Y. Chu, and Z. Ge, Asia-Pac. J. Chem. Eng. **4**, 518–521 (2009).
[15]G. Blasse, J. Inorg. Nucl. Chem. **27**, 993–1003 (1965).
[16]S. Vasala and M. Karppinen, Prog. Solid State Chem. **43**, 1–36 (2015).
[17]M. W. Lufaso and P. M. Woodward, Acta Crystallogr., Sect. B **60**, 10–20 (2004).
[18]R. D. Shannon, Acta Crystallogr., Sect. A **32**, 751–767 (1976).
[19]T. Dey, A. Maljuk, D. V. Efremov, O. Kataeva, S. Gass, C. G. F. Blum, F. Steckel, D. Gruner, T. Ritschel, A. U. B. Wolter, J. Geck, C. Hess, K. Koepernik, J. van den Brink, S. Wurmehl, and B. Büchner, Phys. Rev. B **93**, 014434 (2016).
[20]D. D. Khalyavin, A. M. R. Senos, and P. Q. Mantas, Powder Diffr. **19**, 280–283 (2004).
[21]D. E. Bugaris, J. P. Hodges, A. Huq, and H. C. Zur Loye, J. Solid State Chem. **184**, 2293–2298 (2011).
[22]M. L. Moreira, E. Pairs, G. S. do Nascimento, V. M. Longo, J. R. Sambrano, V. R. Mastelaro, M. I. B. Bernardi, J. Andrés, J. A. Varela, and E. Longo, Acta Mater. **57**, 5174–5185 (2009).
[23]H. L. Feng, M. Arai, Y. Matsushita, Y. Tsujimoto, Y. Guo, C. I. Sathish, X. Wang, Y. H. Yuan, M. Tanaka, and K. Yamaura, J. Am. Chem. Soc. **136**, 3326–3329 (2014).
[24]E. Knittle and R. Jeamloz, Science **235**, 668–670 (1987).
[25]G. Serghiou, A. Zerr, and R. Boehler, Science **280**, 2093–2095 (1998).
[26]J. Oliveira, J. Agostinho Moreira, A. Almeida, V. H. Rodrigues, M. M. R. Costa, P. B. Tavares, P. Bouvier, M. Guennou, and J. Kreisel, Phys. Rev. B **85**, 052101 (2012).
[27]D. A. Mota, A. Almeida, V. H. Rodrigues, M. M. R. Costa, P. Tavares, P. Bouvier, M. Guennou, J. Kreisel, and J. A. Moreira, Phys. Rev. B **90**, 054104 (2014).
[28]M. C. Weber, M. Guennou, H. J. Zhao, J. Íñiguez, R. Vilarinho, A. Almeida, J. A. Moreira, and J. Kreisel, Phys. Rev. B **94**, 214103 (2016).
[29]T. Aoyama, K. Yamauchi, A. Iyama, S. Picozzi, K. Shimizu, and T. Kimura, Nat. Commun. **5**, 4927 (2014).
[30]T. Aoyama, A. Iyama, K. Shimizu, and T. Kimura, Phys. Rev. B **91**, 081107(R) (2015).
[31]Y. Wu, X. Chen, J. Zhang, J. Liu, W. Xiao, Z. Wu, and X. Chen, J. Appl. Phys. **114**, 154110 (2013).
[32]F. Hong, B. Yue, N. Hirao, G. Ren, B. Chen, and H. Mao, Appl. Phys. Lett. **109**, 241904 (2016).
[33]T. K. Koo, S. Lee, and S. W. Cheong, Appl. Phys. Lett. **76**, 224 (2000).
[34]L. Ehm, L. A. Borkowski, J. B. Parise, S. Ghose, and Z. Chen, Appl. Phys. Lett. **98**, 021901 (2011).
[35]H. Hua and Y. K. Vohra, Appl. Phys. Lett. **71**, 2602 (1997).
[36]A. Chandra, Appl. Phys. Lett. **90**, 142903 (2007).
[37]L. Liu, H. X. Song, X. Li, D. Zhang, R. Mathieu, S. Ivanov, H. Skogby, and P. Lazor, Appl. Phys. Lett. **114**, 162903 (2019).
[38]Y. Liu, J. Wang, M. Azuma, W. Mao, and W. Yang, Appl. Phys. Lett. **104**, 043108 (2014).
[39]T. Yamanaka, T. Okada, and Y. Nakamoto, Phys. Rev. B **80**, 094108 (2009).
[40]M. Azuma, S. Carlsson, J. Rodgers, M. G. Tucker, M. Tsujimoto, S. Ishiwata, S. Isoda, Y. Shimakawa, M. Takano, and J. P. Attfield, J. Am. Chem. Soc. **129**, 14433–14436 (2007).
[41]L. Zhang, Y. Meng, P. Dera, W. Yang, W. L. Mao, and H. K. Mao, Proc. Natl. Acad. Sci. **110**, 6292–6295 (2013).
[42]C. Meade, H. K. Mao, and J. Hu, Science **268**, 1743–1745 (1995).
[43]L. Zhang, Y. Meng, W. Yang, L. Wang, W. L. Mao, Q. S. Zeng, J. S. Jeong, A. J. Wagner, K. A. Mkhoyan, W. Liu, R. Xu, and H. K. Mao, Science **344**, 877–882 (2014).
[44]K. Hirose, Y. Fei, Y. Ma, and H. K. Mao, Nature **397**, 53–56 (1999).
[45]Y. Shirako, H. Kojitani, M. Akaogi, K. Yamaura, and E. Takayama-Muromachi, Phys. Chem. Miner. **36**, 455 (2009).
[46]A. M. Glazer, Acta Crystallogr., Sect. B **28**, 3384 (1972).
[47]A. M. Glazer, Acta Crystallogr., Sect. A **31**, 756 (1975).
[48]R. Vilarinho, P. Bouvier, M. Guennou, I. Peral, M. C. Weber, P. Tavares, M. Mihalik, Jr., M. Mihalik, G. Garbarino, M. Mezouar, J. Kreisel, A. Almeida, and J. Agostinho Moreira, Phys. Rev. B **99**, 064109 (2019).
[49]J.-S. Zhou, J. A. Alonso, A. Muoñz, M. T. Fernández-Díaz, and J. B. Goodenough, Phys. Rev. Lett. **106**, 057201 (2011).
[50]R. Haumont, P. Bouvier, A. Pashkin, K. Rabia, S. Frank, B. Dkhil, W. A. Crichton, C. A. Kuntscher, and J. Kreisel, Phys. Rev. B **79**, 184110 (2009).
[51]M. Guennou, P. Bouvier, G. S. Chen, B. Dkhil, R. Haumont, G. Garbarino, and J. Kreisel, Phys. Rev. B **84**, 174107 (2011).
[52]H. J. Xiang, M. Guennou, J. Íñiguez, J. Kreisel, and L. Bellaiche, Phys. Rev. B **96**, 054102 (2017).
[53]P. Chen, M. N. Grisolia, H. J. Zhao, O. E. González-Vázquez, L. Bellaiche, M. Bibes, B. G. Liu, and J. Íñiguez, Phys. Rev. B **97**, 024113 (2018).
[54]J. Zhao, N. L. Ross, and R. J. Angel, Acta Crystallogr., Sect. B **60**, 263 (2004).
[55]R. J. Angel, J. Zhao, and N. L. Ross, Phys. Rev. Lett. **95**, 025503 (2005).
[56]T. Tohei, A. Kuwabara, T. Yamamoto, F. Oba, and I. Tanaka, Phys. Rev. Lett. **94**, 035502 (2005).
[57]N. W. Thomas, Acta Crystallogr., Sect. B **52**, 954 (1996).
[58]M. Avdeev, E. N. Caspi, and S. Yakovlev, Acta Crystallogr., Sect. B **63**, 363 (2007).
[59]V. S. Bhadram, D. Swain, R. Dhanya, M. Polentarutti, A. Sundaresan, and C. Narayana, Mater. Res. Express **1**, 026111 (2014).
[60]P. Bouvier and J. Kreisel, "Pressure-induced phase transition in $LaAlO_3$," J. Phys. **14**, 3981 (2002).
[61]B. J. Kennedy, T. Vogt, C. D. Martin, J. B. Parise, and J. A. Hrilijac, J. Phys. **13**, L925–L930 (2001).
[62]D. Andrault and J. P. Poirier, Phys. Chem. Miner. **18**, 91–105 (1991).
[63]J. Zhao, N. L. Ross, and R. J. Angle, Phys. Chem. Miner. **31**, 299–305 (2004).
[64]T. Ishidate and T. Isonuma, Ferroelectrics **137**, 45–52 (1992).
[65]J. Zhao, N. L. Ross, R. J. Angel, M. A. Carpenter, C. J. Howard, D. A. Pawlak, and T. Lukasiewicz, J. Phys. **21**, 235403 (2009).
[66]B. J. Kennedy, T. Vogt, C. D. Martin, J. B. Parise, and J. A. Hriljac, Chem. Mater. **14**, 2644–2648 (2002).
[67]I. Loa, P. Adler, A. Grzechnik, K. Syassen, U. Schwarz, M. Hanfland, G. K. Rozenberg, P. Gorodetsky, and M. P. Pasternak, Phys. Rev. Lett. **87**, 125501 (2001).
[68]W. M. Xu, O. Naaman, G. K. Rozenberg, M. P. Pasternak, and R. D. Taylor, Phys. Rev. B **64**, 094411 (2001).
[69]N. Li, Y. Li, H. Li, R. Tang, Y. Zhao, D. Han, Y. Ma, Q. Cui, P. Zhu, and X. Wang, Chin. Phys. B **23**, 069101 (2014).
[70]L. Pinsard-Gaudart, J. Rodríguez-Carvajal, A. Daoud-Aladine, I. Goncharenko, M. Medarde, R. I. Smith, and A. Revcolevschi, Phys. Rev. B **64**, 064426 (2001).
[71]A. Y. Ramos, H. C. N. Tolentino, N. M. Souza-Neto, J. P. Itié, L. Morales, and A. Caneiro, Phys. Rev. B **75**, 052103 (2007).
[72]S. Gomez-Salces, F. Aguado, F. Rodrıguez, R. Valiente, J. Gonzalez, R. Haumont, and J. Kreisel, Phys. Rev. B **85**, 144109 (2012).

[73]G. Kh. Rozenberg, M. P. Pasternak, W. M. Xu, L. S. Dubrovinsky, S. Carlson, and R. D. Taylor, Europhys. Lett. **71**, 228 (2005).
[74]M. W. Lufaso, R. B. Macquart, Y. Lee, B. T. Vogta, and H. Loye, Chem. Commun. **2**, 168–170 (2006).
[75]K. S. Wallwork, B. J. Kennedy, Q. Zhou, Y. Lee, and T. Vogt, J. Solid State Chem. **178**, 207–211 (2005).
[76]J. S. Olsena, L. Gerwardb, G. Vaitheeswaranc, V. Kanchanac, and L. Alff, High Pressure Res. **29**, 83–86 (2009).
[77]B. Manoun, J. M. Igartua, M. Gateshki, and S. K. Saxena, J. Mol. Struct. **888**, 244–252 (2008).
[78]B. Manoun, J. M. Igartua, M. Gateshki, and S. K. Saxena, J. Phys. **16**, 8367–8376 (2004).
[79]L. Liu, S. Ivanov, R. Mathieu, M. Weil, X. Li, and P. Lazor, J. Alloys Compd. **801**, 310–317 (2019).
[80]N. Li, B. Manoun, L. Tang, F. Ke, F. Liu, H. Dong, P. Lazor, and W. Yang, Inorg. Chem. **55**, 6770–6775 (2016).
[81]D. Han, W. Gao, N. Li, R. Tang, H. Li, Y. Ma, Q. Cui, P. Zhu, and X. Wang, Chin. Phys. B **22**, 059101 (2013).
[82]S. Meenakshi, V. Vijayakumar, S. N. Achary, and A. K. Tyagi, J. Phys. Chem. Solids **72**, 609–612 (2011).
[83]A. K. Mishra, H. K. Poswal, S. N. Acharya, A. K. Tyagi, and S. M. Sharma, Phys. Status Solidi B **247**, 1773–1777 (2010).
[84]J. Zhao, N. L. Ross, and R. J. Angel, Acta Crystallogr., Sect. B **62**, 431–439 (2006).
[85]M. W. Lufaso, P. W. Barnes, and P. M. Woodward, Acta Crystallogr., Sect. B **62**, 397–410 (2006).
[86]T. Goko, Y. Endo, E. Morimoto, J. Arai, and T. Matsumoto, Physica B **329-333**, 837–839 (2003).
[87]P. Zhao, R. C. Yu, F. Y. Li, and Z. X. Liu, J. Appl. Phys. **92**, 1942 (2002).
[88]Y. Qian, H. Wu, R. Lu, W. Tan, C. Xiao, and K. Deng, J. Appl. Phys. **112**, 103712 (2012).
[89]N. Zu, J. Wang, and Z. Wu, J. Phys. Chem. C **117**, 7231–7235 (2013).
[90]H. Zhao, X. Liu, X. Chen, and L. Bellaiche, Phys. Rev. B **90**, 195147 (2014).
[91]B. J. Kennedy, L. Li, Y. Lee, and T. Vogt, J. Phys. **16**, 3295–3301 (2004).
[92]P. Adler, S. A. Medvedev, P. G. Naumov, S. Mohitkar, R. Rüffer, M. Jansen, and C. Felser, Phys. Rev. B **99**, 134443 (2019).
[93]L. S. I. Veiga, G. Fabbris, M. van Veenendaal, N. M. Souza-Neto, H. L. Feng, K. Yamaura, and D. Haskel, Phys. Rev. B **91**, 235135 (2015).
[94]J.-S. Zhou, J. B. Goodnough, and B. Dabrowski, Phys. Rev. Lett. **94**, 226602 (2005).
[95]H. Kobayashi, S. Ikeda, Y. Yoda, N. Hirao, Y. Ohishi, J. A. Alonso, M. J. Martinez-Lope, R. Lengsdorf, D. I. Khomskii, and M. M. Abd-Elmeguid, Phys. Rev. B **91**, 195148 (2015).
[96]Y. Wang, J. Ying, Z. Zhou, J. Sun, T. Wen, Y. Zhou, N. Li, Q. Zhang, F. Han, Y. Xiao, P. Chow, W. Yang, V. V. Struzhkin, Y. Zhao, and H. K. Mao, Nat. Commun. **9**, 1914 (2018).
[97]Y. Wang, Z. Zhou, T. Wen, Y. Zhou, N. Li, F. Han, Y. Xiao, P. Chow, J. Sun, M. Pravica, A. L. Cornelius, W. Yang, and Y. Zhao, J. Am. Chem. Soc. **138**, 15751–15757 (2016).
[98]T. Wen, Y. Wang, N. Li, Q. Zhang, Y. Zhao, W. Yang, Y. Zhao, and H. K. Mao, J. Am. Chem. Soc. **141**, 505 (2019).
[99]N. Li, F. Fan, F. Sun, Y. Wang, Y. Zhao, F. Liu, Q. Zhang, D. Ikuta, Y. Xiao, P. Chow, S. M. Heald, C. Sun, D. Brewe, A. Li, X. Lü, H. Mao, D. I. Khomskii, H. Wu, and W. Yang, Phys. Rev. B **99**, 195115 (2019).
[100]G. R. Hearne, M. P. Pasternak, R. D. Taylor, and P. Lacorre, Phys. Rev. B **51**, 11495 (1995).
[101]V. V. Bannikov, I. R. Shein, V. L. Kozhevnikov, and A. L. Ivanovskii, J. Struct. Chem. **49**, 781 (2008).
[102]F. Aguado, F. Rodríguez, R. Valiente, J. Itiè, and M. Hanfland, Phys. Rev. B **85**, 100101(R) (2012).
[103]Z. Chen, T. A. Tyson, K. H. Ahn, Z. Zhong, and J. Hu, J. Magn. Magn. Mater. **322**, 3049–3052 (2010).
[104]C. Meneghini, D. Levy, S. Mobilio, M. Ortolani, M. Nuñez-Reguero, A. Kumar, and D. D. Sarma, Phys. Rev. B **65**, 012111 (2001).
[105]J.-G. Cheng, J.-S. Zhou, J. B. Goodenough, J. A. Alonso, and M. J. Martinez-Lope, Phys. Rev. B **82**, 085107 (2010).
[106]X. Wang, Q. Cui, Y. Pan, W. Gao, J. Zhang, and G. Zou, J. Alloys Compd. **321**, 72–75 (2001).
[107]K. Kugel and D. I. Khomskii, Sov. Phys. Usp. **25**, 231 (1982).
[108]R. Pradhees, H. S. Nair, V. Sankaranarayanan, and K. Sethupathi, Eur. Phys. J. B **85**, 260 (2012).
[109]T. Kawamoto, K. Fujita, I. Yamada, T. Matoba, S. J. Kim, P. Gao, X. Pan, S. D. Findlay, C. Tassel, H. Kageyama, A. J. Studer, J. Hester, T. Irifune, H. Akamatsu, and K. Tanaka, J. Am. Chem. Soc. **136**, 15291–15299 (2014).
[110]C. Moure and O. Peña, Prog. Solid State Chem. **43**, 123–148 (2015).
[111]A. A. Belik, T. Furubayashi, Y. Matsushita, M. Tanaka, S. Hishita, and E. Takayama-Muromachi, Angew. Chem., Int. Ed. **48**, 6117–6120 (2009).
[112]P. Adler, U. Schwarz, and K. Syassen, J. Solid State Chem. **155**, 381–388 (2000).
[113]F. Zhu, Y. Wu, X. Lai, S. Qin, K. Yang, J. Liu, and X. Wu, Phys Chem. Miner. **41**, 449–459 (2014).
[114]T. Kawakami, S. Nasu, K. Kuzushita, T. Sasaki, S. Morimoto, T. Yamada, S. Endo, S. Kawasaki, and M. Takano, J. Phys. Soc. Jpn. **72**, 33–36 (2003).
[115]N. L. Ross, R. J. Angel, and F. Seifert, Phys. Earth Planet. Inter. **129**, 145–151 (2002).
[116]I. Yamada, S. Marukawa, M. Murakami, and S. Mori, Appl. Phys. Lett. **105**, 231906 (2014).
[117]Y. Long, T. Kawakami, W. Chen, T. Saito, T. Watanuki, Y. Nakakura, Q. Liu, C. Jin, and Y. Shimakawa, Chem. Mater. **24**, 2235–2239 (2012).
[118]A. Möller, U. Löw, T. Taetz, M. Kriener, G. André, F. Damay, O. Heyer, M. Braden, and J. A. Mydosh, Phys. Rev. B **78**, 024420 (2008).
[119]D. A. Vander Griend, S. Boudin, V. Caignaert, K. R. Poeppelmeier, Y. Wang, V. P. Dravid, M. Azuma, M. Takano, Z. Hu, and J. D. Jorgensen, J. Am. Chem. Soc. **121**, 4787–4792 (1999).